Mon. Not. R. Astron. Soc. **351,** 101–109 (2004) doi:10.1111/j.1365-2966.2004.07757.x

A binary system of tailed radio galaxies

I. Klamer,[1]★ R. Subrahmanyan[2] and R. W. Hunstead[1]

[1]*School of Physics, University of Sydney, Sydney, NSW 2006, Australia*
[2]*Australia Telescope National Facility, CSIRO, Locked Bag 194, Narrabri NSW 2390, Australia*

Accepted 2004 February 19. Received 2004 February 4; in original form 2003 September 29

ABSTRACT

We present a detailed study of a binary system of tailed radio galaxies which, along with 3C 75, is the only such binary known to exist. The binary is located in a region of low galaxy density at the periphery of a poor cluster Abell S345, but lies close to the massive Horologium–Reticulum supercluster. The radio sources have bent-tail morphologies and show considerable meandering and wiggling along the jets, which are collimated throughout their lengths. This work presents observations of the large-scale-structure environment of the binary tailed radio sources with a view to examining the influence of large-scale flows on the morphology and dynamics of the associated radio tails. We argue that the orbital motions of the host galaxies together with tidal accelerations toward the supercluster have resulted in the complex structure seen in these radio tails.

Key words: galaxies: interactions – galaxies: jets – large-scale structure of Universe – radio continuum: galaxies.

1 INTRODUCTION

Narrow-angle tailed (NAT) radio sources or head–tail (HT) sources consist of twin jets issuing from the active nuclei in some galaxies and then bending by an angle of almost 90°. These sources are usually found in rich cluster environments, where the jets are understood to have been swept back by the deflecting pressure of the dense intracluster medium (ICM) arising from the relative motion between the host galaxy and that medium. Studies have shown that to bend these tails, the ICM must be hot and dense and the relative velocity between the radio galaxy and the ICM must be of order 1000 km s^{-1} (Venkatesan et al. 1994). These required velocities and densities make it unlikely for NATs to exist in low-density environments.

Wide-angle tail (WAT) radio sources, alternatively, have beams which typically bend through angles less than 90°. These sources are, once again, usually found in rich clusters; however, the WATs are usually associated with a dominant galaxy – often the central galaxy – which is not expected to be moving at high speeds with respect to the ambient medium. Therefore, the cause for their bending has been unclear: motions of the parent galaxy with respect to the ICM; buoyancy of the relatively light synchrotron plasma in the ICM thermal gas; weather/turbulence in the ICM associated with dynamical evolution; and cluster–cluster mergers/interactions may all play roles in particular circumstances.

In this paper we do not attempt to subclassify the tailed radio galaxies into WAT and NAT sources because the distinction might sometimes be confused by projection effects. Instead, we refer to them simply as bent-tail (BT) sources.

★E-mail: klamer@physics.usyd.edu.au

Comparisons between the radio morphologies of BT sources in cluster environments and the distribution of the intracluster thermal gas as seen, for example, in X-ray images, indicate that the thermal gas is almost always asymmetric and aligned towards the direction of the bending (Gomez et al. 1997). It is currently believed that these clusters are undergoing mergers, resulting in large-scale flows of hot gas owing to the changing gravitational potential. The bending of the BTs is a consequence of these flows. BTs in merging clusters are, therefore, diagnostic of the ICM weather and, consequently, of the evolving gravitational potential resulting from the merger.

Our attention was drawn to the unusual nature of the radio source J0321−455 when it appeared in the field of the giant radio galaxy PKS B0319−454 (Saripalli, Subrahmanyan & Hunstead 1994) with a four-leaf-clover structure. Follow-up observations at higher resolution revealed the source to have an extremely unusual configuration: as shown in the overview in Fig. 1, J0321−455 is a close pair of twin-tailed radio galaxies associated with what appears to be a binary galaxy system. We label the northern radio galaxy J0321−455N and the southern source J0321−455S. The other optical objects in the field of Fig. 1 are labelled alphabetically and discussed in Section 2.3. The system is located in a region of low galaxy density, at the periphery of the poor Abell cluster S345 (Abell, Corwin & Olowin 1989; ACO), and in the vicinity of the massive Horologium–Reticulum (H–R) supercluster. The directions toward S345 and the supercluster are indicated in the figure.

The radio tails in J0321−455 are probably a result of, and a diagnostic for (i) the motions of the host ellipticals about their centre of mass and (ii) the relative motion of the binary with respect to the intergalactic thermal plasma as a result of the gravitational potentials of the large-scale structure. Therefore, we have undertaken a study of the radio structures and the large-scale galaxy environment

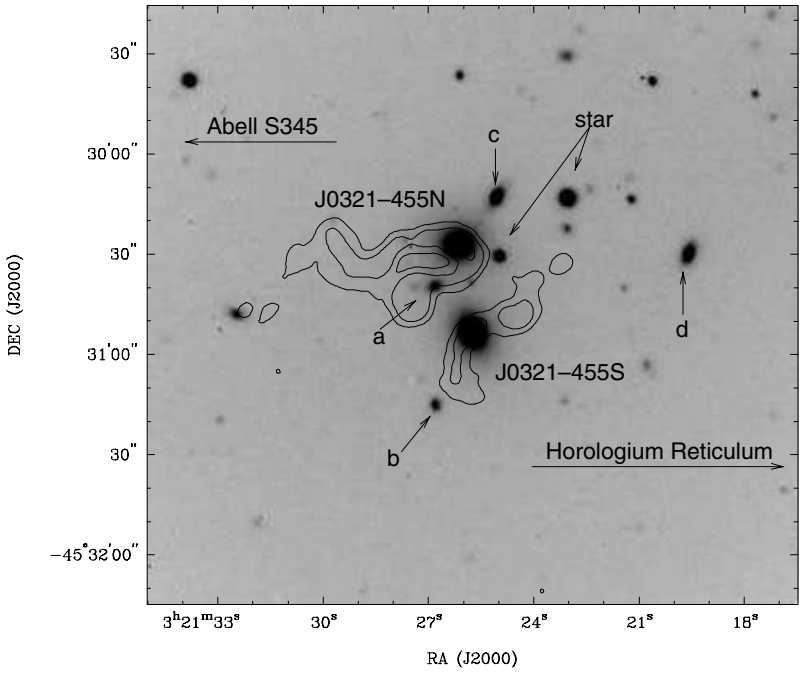

Figure 1. The binary radio galaxies J0321−455N and J0321−455S. 2.4-GHz radio contours are overlaid on a combined *R*- and *V*-band optical image of the field made using the ANU 2.3-m telescope. The contours correspond to 4, 16, 64 and 128 times the rms image noise of 60 μJy beam^{-1}. Spectroscopy (see Table 2) reveals that the objects labelled c and d and the radio galaxies are at about the same redshift.

in this unique situation with the aim of understanding the roles of gas and galaxy dynamics in the triggering and formation of BTs. In this paper we present radio and optical observations of the binary system and its large-scale environment. Our aim was to image the tailed radio structures and understand the large-scale mass distribution to infer the dynamics and kinematics of the system. The determination of dynamical and spectral ages are inputs to understanding how the nuclear activity in both members of this binary system might have been triggered and fuelled. The paper is structured as follows: Section 2 describes the multiwavelength observations which include high-resolution radio imaging, spectroscopy of the nearby objects in Fig. 1 and the brightest members of S345, and multifibre spectroscopy of a 2° field to map the 3-dimensional (3D) large-scale structure. Section 3 presents a discussion wherein we have developed constraints on the source formation based on the observational data on the radio structures and the large-scale environment. Throughout the paper we adopt the following cosmological parameters: $\Omega_\Lambda = 0.7$; $\Omega_m = 0.3$; and $H_0 = 71$ km s^{-1} Mpc^{-1}. S345 and the binary galaxy system are at a mean redshift of about $z = 0.07$ and at this distance, 1 arcmin corresponds to a linear size of 79 kpc.

2 OBSERVATIONS

2.1 Radio observations

The binary tailed radio sources J0321−455N and J0321−455S were observed with the Australia Telescope Compact Array (ATCA) at 1.4, 2.4, 4.8 and 8.6 GHz; a journal of the radio observations is given in Table 1. The flux density scale in all cases was set using observations of PKS B1934−638; the time variations in the complex antenna gains as well as the bandpass were calibrated using frequent observations of a nearby unresolved calibrator, B0332−403. The visibility data were calibrated and imaged using MIRIAD following standard ATCA data reduction procedures (Sault & Killeen 1999). The beam FWHM sizes and the rms noise in the final continuum images made at the different observing frequencies are listed in Table 1. The Stokes I radio images at 1.4, 4.8 and 8.6 GHz are shown in Figs 2, 3 and 4, All radio images displayed here and used in the analysis were corrected for the attenuation caused by the telescope primary beam. The centres of the optical hosts are shown marked with crosses in all three images.

Table 1. Journal of radio observations made with the ATCA and the parameters of the radio images produced therefrom.

	1.4 GHz	2.4 GHz	4.8 GHz	8.6 GHz
Observing epoch	2001 May & Aug	2001 May & Aug	1992 Oct	1992 Oct
Array configurations	6A, 6B	6A, 6B	6C	6C
Obs. time (h)	2 × 12	2 × 12	12	12
Synthesized beam (arcsec^2)	7.7 × 5.4	5.0 × 4.2	3.9 × 2.6	1.3 × 0.8
	at PA −1.°8	at PA −8.°8	at PA −15.°0	at PA −9.°5
Continuum image rms noise (μJy beam^{-1})	64	60	68	60
Flux density of J0321−455N (mJy)	111	63	38	4
Flux density of J0321−455S (mJy)	41	22	13	5

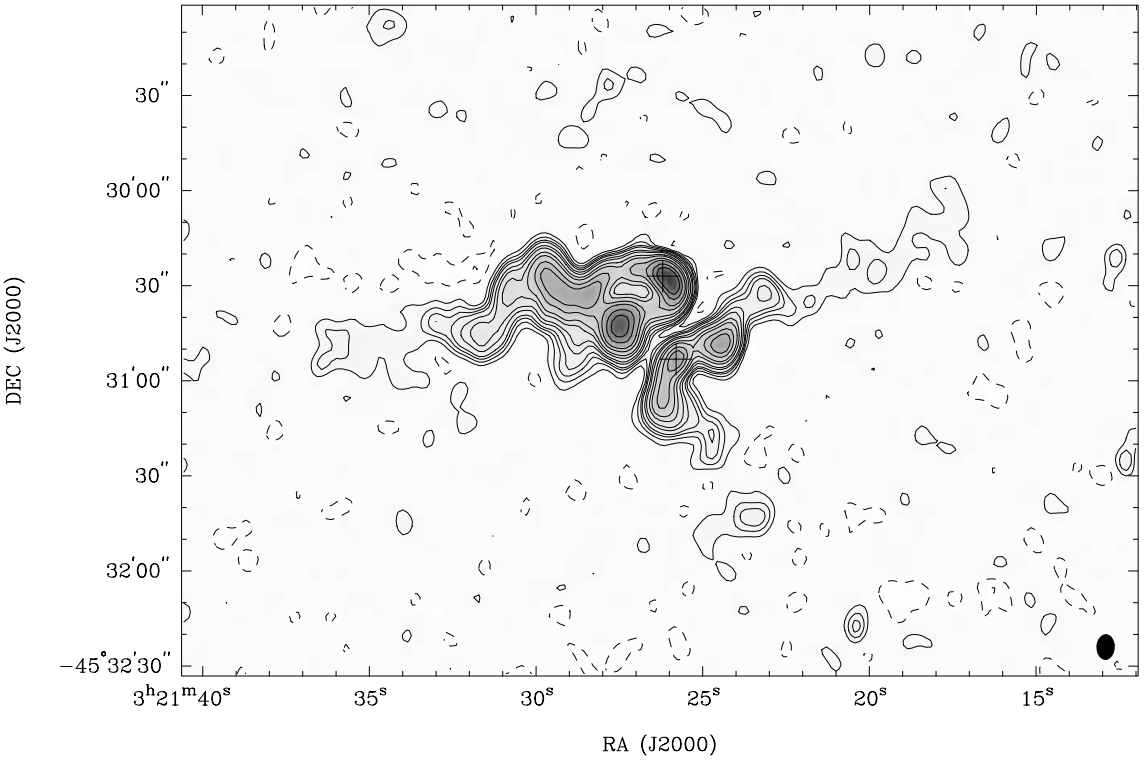

Figure 2. 1.4-GHz total intensity image. This image, and the following radio images, has been corrected for the primary beam attenuation. Additionally, the positions of the centres of the host optical galaxies are marked with crosses and the beam FWHM sizes are shown using filled ellipses at the bottom right corners. Contour levels are at ±1, ± 2, 3, 4, 6, 8, 12, 16, 24, 32, 48 and 64 × 0.12 mJy beam^{-1}; the lowest contour is twice the image rms noise.

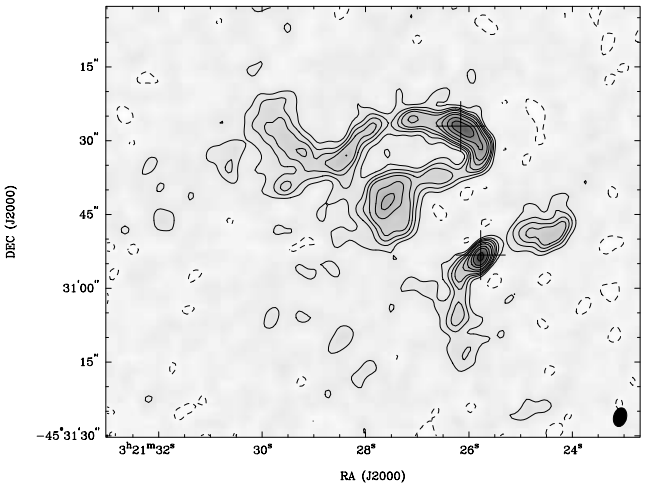

Figure 3. 4.8-GHz total intensity image. Contour levels are shown at ±1, ±2, 3, 4, 6, 8, 12, 16 and 24 × 0.15 mJy beam^{-1}; the lowest contour is about twice the image rms noise.

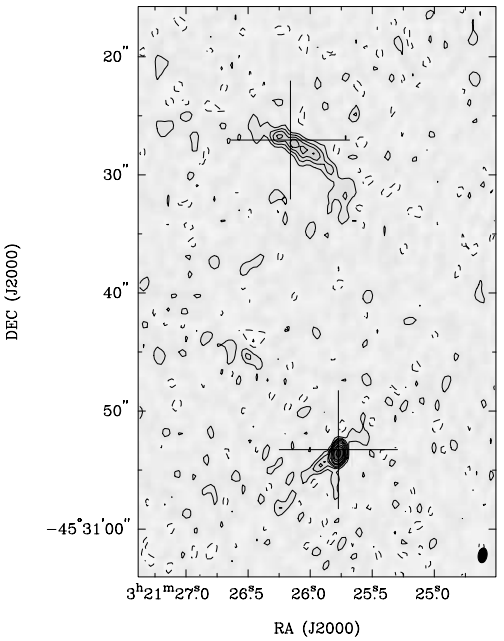

Figure 4. 8.6-GHz total intensity image. Contour levels are at ±1, ± 2, 3, 4, 6, 8, 12, 16, 24 × 0.12 mJy beam^{-1}; the lowest contour is about twice the image rms noise.

The images at the different frequencies and resolutions show complex structure in the radio tails of both J0321−455N and J0321−455S. The tails of both radio sources appear as collimated jets that undergo numerous sharp bends and wiggles as they trail away from their host galaxy. At 1.4 GHz, the radio tails have been detected out to projected linear distances of 200 and 150 kpc in J0321−455N and J0321−455S, respectively.

The surface brightness is a maximum at the locations of the optical hosts and decreases away from the centres as expected for Fanaroff–Riley class I sources (FR I; Fanaroff & Riley 1974). The jets in J0321−455N appear, in projection, to bend and almost form a closed loop and then bend sharply in opposing directions; the overall structure in the inner parts is Ω shaped as seen clearly in the

4.8-GHz image. The south-east jet in J0321−455N appears to end in a plume of higher surface brightness: this structure might simply be a collimated tail viewed close to the line of sight. J0321−455S, alternatively, displays more typical WAT morphology. The jets from this source bend to the same side and the inner part of this source, as seen in the 4.8-GHz image, has a C-shaped morphology. A fascinating feature (as seen, for example, in Hardcastle & Sakelliou 2004) of both these BT sources is the sudden drop in surface brightness that occurs about two-thirds to half of the distance to the ends of the tails. These lower surface brightness extensions are clearly seen in the 1.4-GHz image but are not detected in the higher frequency images. There is considerable meandering in the jet flow path and fairly abrupt changes in direction in these extensions. The collimation in the radio jets appears to be maintained and there is no evidence for any flaring or transition to wider flows throughout in spite of the sharp changes in direction.

In our highest resolution images at 8.6 GHz, all of the extended tails fall below the sensitivity of the detectors and the only compact structures detected at this high frequency are a bright core coincident with the centre of the galaxy associated with J0321−455S and a bright rim representing the inner jets at the centre of J0321−455N. The core of J0321−455S is unresolved and has a deconvolved size of <0.3 arcsec and a flux density of 3.76 mJy at 8.6 GHz.

The total flux density of J0321−455, as computed from the ATCA images, is 152 and 85 mJy at 1.4 and 2.4 GHz, respectively. The flux densities are 330 and 230 mJy at 408[1] and 843 MHz, respectively; the PMN survey (Griffith et al. 1994) lists the source flux-density as being 60 mJy at 4.85 GHz. The sources are at a luminosity distance of 318 Mpc and at 1.4 GHz, the radio powers of J0321−455N and J0321−455S are 1.3×10^{24} and 4.8×10^{23} W Hz^{-1}, respectively. These low luminosities are consistent with their FR I type structure.

2.1.1 Spectral index

The overall spectral index of the source, α, is ∼0.8 between 843 MHz and 1.4 GHz (we adopt the definition $S_\nu \propto \nu^{-\alpha}$). However, the total spectrum is flatter at lower frequencies with $\alpha \approx 0.5$ between 408 and 843 MHz.

To compute the spectral index distribution between 1.4 and 2.4 GHz we smoothed the images to a common beam of 8.2 arcsec × 6.6 arcsec at a position angle of $-6\overset{\circ}{.}0$. The spectrum is flattest towards the optical hosts of the two-tailed radio sources; towards the centre of J0321−455N α is within the range 0.15–0.25 and towards the centre of J0321−455S α is in the range 0–0.1. J0321−455S has a compact core that is unresolved in our highest resolution observations and the spectral index is also the flattest towards this core, implying it may still be active. Both galaxies also show a steepening in the two-point spectral index away from their centres and along their radio tails. This trend is consistent with their FR I structure. The spectral index takes on values in the range 0.3–1.0 in the higher surface brightness tails that are visible in the 4.8-GHz image and steepens further to 1.0–2.0 in the low-surface-brightness extensions that are detected in the 1.4-GHz image.

2.1.2 Rotation measure and polarization

We have computed the distribution in rotation measure (RM) over the two radio galaxies using the 1.4 and 2.4-GHz position angle images, ignoring $n\pi$ ambiguities. We measured the RM for regions whose Stokes Q and U signal-to-noise ratios were each greater than 2.0 and whose Stokes I signal-to-noise ratios were greater than 2.5 and where the formal error in position angle was less than 10°.

The RM distribution in J0321−455S lies within the range 0 to –10 rad m^{-2} (corresponding to a maximum rotation angle of 8° at 2.4 GHz) over the eastern tail and optical galaxy positions. However, the RM distribution in the local peak in the western tail of J0321−455S varies steadily across this component by ∼40 rad m^{-2}. The RM distribution in J0321−455N lies within the range ±20 rad m^{-2} (corresponding to a maximum rotation angle of ±16° at 2.4 GHz) over the entire structure and, in the vicinity of the optical host, is observed to vary monotonically through ∼40 rad m^{-2} across the central component.

The RM resulting from the Galactic foreground in the direction of these sources is estimated to be around ±5 rad m^{-2}. The fractional polarization of the radio tails is about 7–13 per cent towards the centres (and optical hosts) and rises along the tails, exceeding 60 per cent at the ends of the detected tails. The projected *B* field along the northern tail of J0321−455N, and the western tail of J0321−455S, appear consistently orthogonal to the direction of jet flow, as is usually the case in FR I radio galaxies. The *B* field appears parallel to the direction of flow in the shorter southern jet of J0321−455S and becomes complicated in the tight knot of the southern tail of J0321−455N where we believe the tail bends into our line of sight.

2.2 Anglo-Australian Telescope spectroscopy of S345

Anglo-Australian Telescope (AAT) service spectroscopy of J0321−455N, J0321−455S and the six brightest members of S345 were obtained on 1999 October 17 using the MITLL2 detector on the RGO spectrograph. Data reduction was performed using routines within the software package FIGARO. Wavelength calibration was achieved by fitting a fifth-order polynomial to short observations of a CuAr comparison lamp. The spectral resolution was 5.4 Å FHWM corresponding to an equivalent velocity resolution of 300 km s^{-1} at 5500 Å. Redshifts were measured and we found that the radio galaxies are located close to the mean redshift ($\bar{z} = 0.0709 \pm 0.0005$) of S345.

2.3 Australian National University 2.3-m observations

Spectroscopic observations of the sources labelled in Fig. 1 were obtained using the Dual Beam Spectrograph on the Australian National University (ANU) 2.3-m telescope at Siding Spring Observatory in 2002 January. The spectra were reduced using FIGARO. Wavelength calibration was computed by fitting a third-order polynomial, with rms residuals of 0.08 Å, to short exposures of a CuAr comparison lamp. The resolutions of the final spectra were determined to be 5.7 (or 387 km s^{-1} at 4500 Å) and 4.3 Å(or 172 km s^{-1} at 7500 Å) for the blue and the red, respectively. The redshifts of each target were determined by cross-correlation with template spectra of known redshift using the methods of Tonry & Davis (1979). We used nine templates consisting of absorption and emission-line galaxy and stellar spectra: these templates were prepared for the 2-degree Field Galaxy Redshift Survey [2dFGRS; Colless (1998)]. Regions containing atmospheric emission and absorption lines were systematically ignored. The adopted redshift of each source was chosen by selecting the template producing the strongest resultant peak in the cross-correlation and smallest error. Table 2 lists the target sources for the observations and their measured redshifts. Galaxies c and

[1] 408-MHz flux-density measurements based on a re-analysis of the Molonglo Cross archival data by Crawford (private communication).

Table 2. Optical properties of the binary galaxies and their close neighbours on the sky. Positions and magnitudes are as measured from ANU 2.3-m images and photometry; redshifts are derived from ANU 2.3-m spectroscopy. The galaxy type *abs* signifies an absorption-line spectrum and *em* an emission-line spectrum.

Object	Mag (V)	RA (J2000)	Dec. (J2000)	Exposure time for the spectra ($\times 10^3$ s)	Redshift (z) $\Delta z = 0.0001$	Type
J0321−455N	15.79	$03^h21^m26\overset{s}{.}2$	–45° 30′ 27″	8	0.0717	*abs*
J0321−455S	15.59	$03^h21^m25\overset{s}{.}8$	–45° 30′ 53″	12	0.0711	*abs*
a	18.90	$03^h21^m26\overset{s}{.}8$	–45° 30′ 40″	4	0.1814	*em*
b	19.26	$03^h21^m26\overset{s}{.}8$	–45° 31′ 15″	6	0.1817	*em*
c	17.73	$03^h21^m25\overset{s}{.}1$	–45° 30′ 13″	4	0.0700	*abs*
d	17.84	$03^h21^m19\overset{s}{.}6$	–45° 30′ 30″	4	0.0704	*abs*

d lie 340 km s^{-1} blueward of the radio galaxies, while a and b are background galaxies.

R and *V* images were also obtained on the 2.3-m telescope. Photometric calibration was tied to observations of the Landolt photometric standard star 95−330 and using the IRAF DAOPHOT analysis package for off-line calibration. The corrected *V* magnitudes are listed in Table 2.

2.4 AAT 2dF multifibre spectroscopy

A SUPERCOSMOS-generated catalogue (using the on-line option to separate stars from galaxies) shows S345 to be located in a region that is densely populated within 1° to its west and sparsely populated within 1° to its east. To explore this larger region, multifibre spectra with a single pointing centre at (J2000) RA $03^h18^m0\overset{s}{.}0$ Dec. −45°30′0.″0 were obtained at the AAT in 2002 January. A magnitude-limited ($16 < B_J < 19.5$) sample of galaxies was obtained from the SUPERCOSMOS catalogue totalling 660 sources. The sample was reduced to 400 using the *B*–*R* colour–magnitude relationship for clusters which uses an estimate of photometric redshifts to reduce contamination from foreground and background galaxies (Gladders & Yee 2000). The optimal configuration of fibres resulted in 327 allocations, 25 of which were used as sky calibrators. The data were reduced using the standard automatic 2dF data reduction program and spectroscopic redshifts were measured with a code written for the 2dFGRS. Of the 302 target sources, 13 were misclassified foreground stars and another 13 produced spectra too poor to estimate reliable redshifts.

2.5 Spectroscopic analysis

The redshift distribution of the remaining 276 galaxies is displayed in the histogram shown in Fig. 5. We searched the distribution for the presence of subgroupings using the KMM alogorithm ('Kayes' mixture model; Ashman, Bird & Zepf 1994) which fits a user-specified number of Gaussian profiles to a data set and assesses the improvement of the fit over a single Gaussian distribution. Employing the algorithm over the range $0.070 < z < 0.085$, and testing for two- and three-component Gaussian fits we found the data to be trimodal with 99.8 per cent confidence. These groups, which indicate a distortion of the local Hubble flow, are hereafter referred to as G1, G2 and G3 as shown in the inset to Fig. 5.

Next, we prepared galaxy distribution plots over the redshift range covering G1, G2 and G3. This distribution is conveyed in Fig. 6 where we plot galaxies as symbols according to their group redshift; galaxies belonging to G1 we plot as stars, G2 as squares and G3 as circles. The most striking feature we see is that G1, which includes the radio galaxies and S345, appears to lie along an

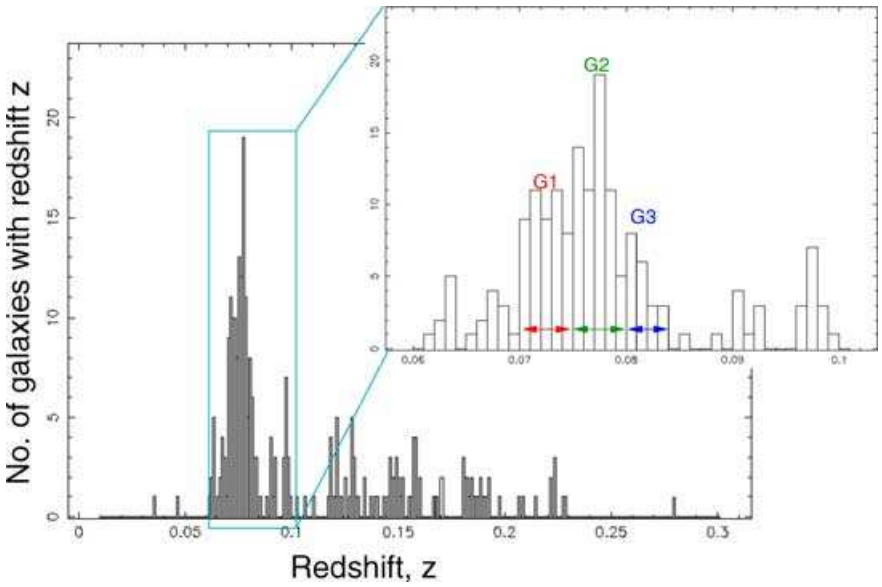

Figure 5. 2dF redshift distribution histogram. Inset shows the trimodal population determined using the KMM algorithm.

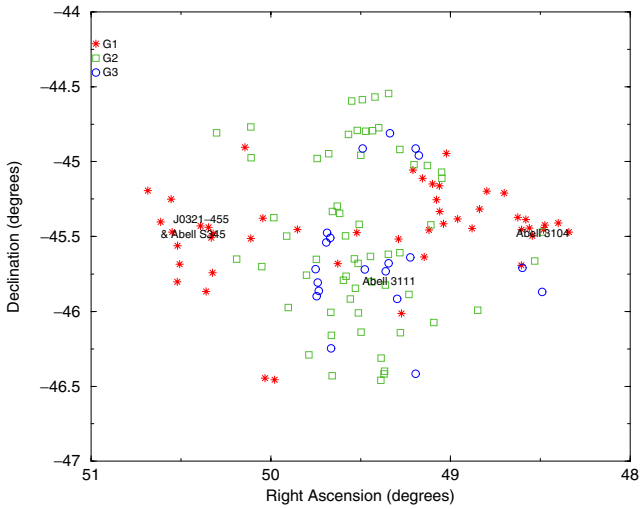

Figure 6. Galaxy distribution over the redshift range containing the G1, G2 and G3 galaxy groups shown in Fig. 5. The galaxies are represented as symbols according to their measured redshift; G1 ($0.070 \leqslant z < 0.075$) as stars, G2 ($0.075 \leqslant z < 0.080$) as squares, and G3 ($0.080 \leqslant z < 0.085$) as circles. Marked are the approximate locations of several known ACO clusters in the field; refer to Table 3 for an exhaustive list including published redshifts.

Table 3. List of clusters associated with the region surrounding J0321−455 with published redshifts and/or distance classes which fall within G1, G2 or G3 identified in Fig. 5.

Cluster	Redshift/Distance Class	Group category
ACO S345	0.070	G1
APM 031555−444222	0.076	G2
ACO S336	0.074	G1
APM 366, ACO S334	0.075, $D = 4$	G2
LCLG −45 113, APM 362	0.071, 0.072	G1
ACO A3104, LCLG −45 112	0.073, 0.073	G1
ACO A3111, APM 367	0.0775, 0.080	G2
ACO S335	$D = 4$	G2

east–west filamentary structure whilst the galaxies within G2 and G3 lie along a plane almost orthogonally to the G1 distribution. For easy reference we also mark the approximate location of the radio galaxies, S345 and a few other known ACO clusters. Known APM (Dalton et al. 1997) and ACO clusters in this region are listed in Table 3 along with their published redshift and the group, according to our definition, which the cluster resides within.[2] For example, Abell 3111 at $z = 0.0775$ resides within G2, whereas Abell 3104 at $z = 0.073$ resides within G1. As a side point, Abell 3111 and 3104 are both known members of the H–R supercluster.

The structure along the north–south axis consists solely of galaxies within G2 and G3 whereas the galaxy overdensities residing mostly east–west consist almost completely of G1 galaxies (which include the radio galaxies). Following the analysis of Rose et al. (2002), a true filament oriented directly north–south should be tightly localized in an RA–z plot but appear as a vertical line in a Dec.–z plot and a filament oriented east–west will show exactly the opposite. A candidate group, alternatively, must be localized in both plots to be physical. We prepared position–velocity plots to establish whether the apparent associations could be physical entities. These are shown in Fig. 7 and clearly illustrate that the three groups do appear to be drawn from three separate filamentary structures, where G2 and G3 are oriented north–south (and are physically separate populations) and G1 east–west.

[2] Where a cluster and/or group has two identifications, both clusters are listed in Table 3.

3 DISCUSSION

den Hartog (1997) defines galaxies located within rich clusters with a velocity difference of $\leqslant 300\,\mathrm{km\,s^{-1}}$ and a projected spatial separation of $\leqslant 70$ kpc to be binary systems. J0321−455N and J0321−455S have a projected separation of 36 kpc and a velocity difference of 180 km s^{-1}, suggesting that they constitute a gravitationally bound binary system.

Notwithstanding the present case, tailed radio sources are extremely uncommon and particularly unusual when they come as a pair. In fact, to our knowledge no other binary system of tailed radio galaxies exist (with the possible exception of 3C 75). It is therefore strongly suggested that the sources are not independent but that each has been influenced by the presence of the other. Our observational evidence to support this suggestion includes the elongation of J0321−455S along an axis oriented toward J0321−455N and the strong probability that the pair constitute a bound binary system with projected geometry suggestive of clockwise orbital motion.

3.1 Connection between the H–R supercluster, S345 and the radio galaxy pair

The data presented in Figs 6 and 7 suggest that S345 is part of a filament extending east–west and intersecting the dominant cluster A3111. There is another filament containing several known clusters extending north–south intersecting A3111. Filamentary structures similar to those we observe have been seen in large-scale redshift surveys (Peacock et al. 2001) and are expected from simulations of large-scale structure. As A3111 is a member of the H–R supercluster, it is presumably close to the bottom of the local gravitational potential. The east–west filament containing S345 and the binary galaxy might be the path along which galaxies flow (gravitationally) towards the deep local potential well close to A3111. The filamentary nature of the structure containing S345 and the binary galaxy is probably a consequence of the tidal forces along the filament and we expect that the binary leads S345 in its infall to the west and towards A3111. The differential acceleration would imply that the binary currently has a greater velocity to the west in comparison with S345. The intergalactic medium (IGM) would also experience the same tidal acceleration and would be drawn into the same filamentary structure traced by the galaxies. In this scenario, the binary might have been tidally torn from S345 during the infall.

Fig. 8 shows the broadband *ROSAT* Position Sensitive Proportional Counter (PSPC) contours (archive image rp800303n00) in the region containing S345. The observation was centred on the ACO cluster A3111. S345, which lies almost 1° from A3111, therefore lies near the edge of the the field of view of the PSPC detector where the point-spread function is significantly distorted. Nevertheless, this poor cluster clearly shows X-ray substructure implying that it is not a relaxed system. More significant is the detection of X-ray gas associated with the binary system and the suggestion of a bridge between the gas associated with S345 and the binary. The structure in the gas is consistent with our interpretation that the binary has been tidally detached from S345 and, along with its gaseous environment, leads S345 in its westward accelerated motion.

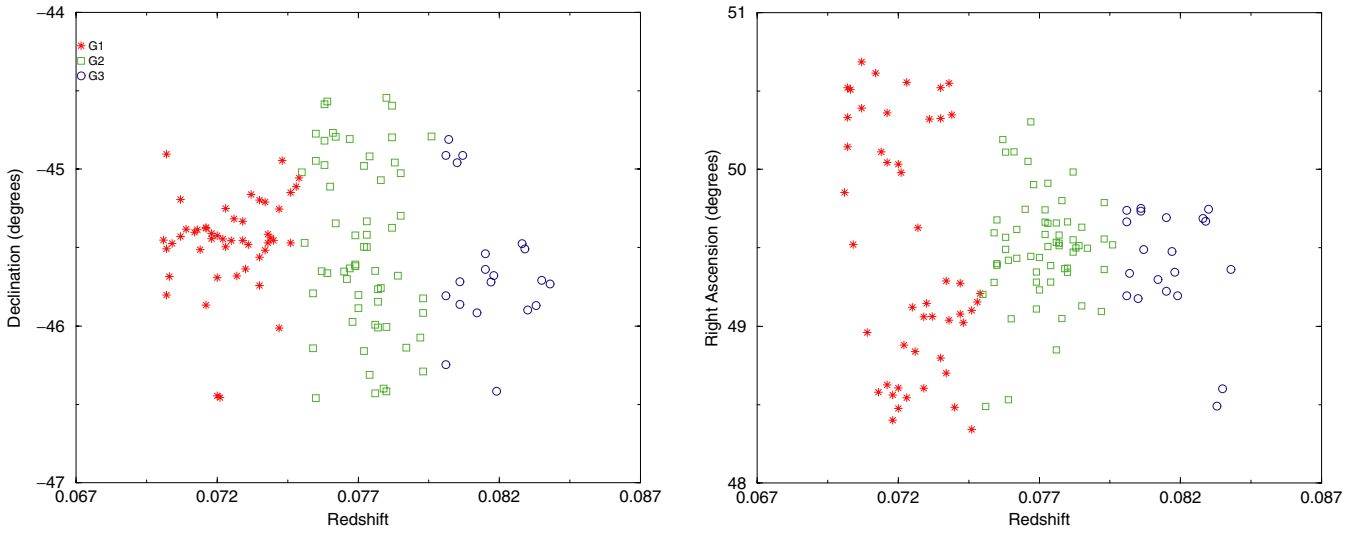

Figure 7. Position–redshift plots with the established groups of G1, G2 and G3 identified.

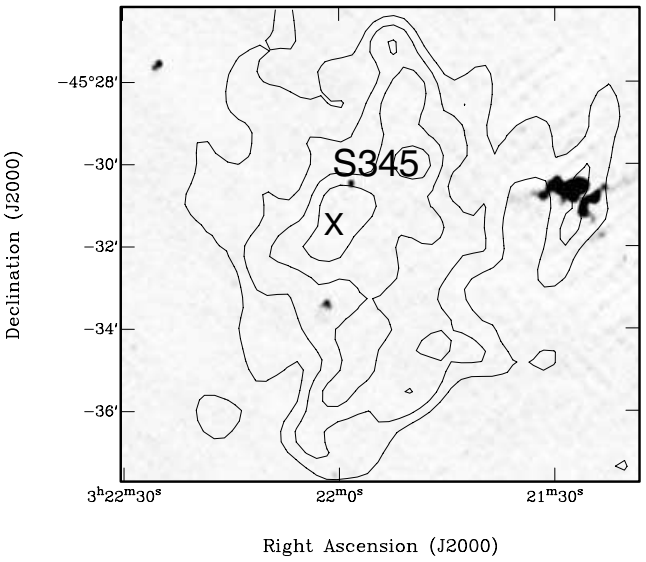

Figure 8. Smoothed (Gaussian of FWHM 60 arcsec) *ROSAT* PSPC X-ray contours overlaid on 20-cm radio image.

3.2 What triggered the radio emission?

Galaxy–galaxy interactions play a vital role in providing fuel to the central black hole of an elliptical galaxy through a nuclear starburst. This starburst can produce enough cold gas to increase the accretion rates surrounding a black hole and trigger nuclear activity (Byrd & Valtonen 1990; Lim et al. 2000; Barton Gillespie, Geller & Kenyon 2003). The presence of close neighbours might, therefore, trigger a starburst and initiate/restart nuclear activity from J0321−455. An obvious interpretation for this system is therefore that both radio galaxies were triggered as a result of the mutual interaction between the massive ellipticals as they travel on close orbits and hence the AGN have a common triggering time. This is consistent with our observations which show the spectral indices along the tails of the pair of galaxies are similar.

Despite the natural conclusion that the radio emission was triggered by galaxy–galaxy interactions, we stress that there are much higher density systems where the incidence of powerful emission is almost non-existent. For example, the high densities in Hickson compact groups (we refer the reader to the review by Hickson 1997) make them ideal regions to search for signs of galaxy interactions. Studies of such groups would therefore be expected to show large numbers of powerful radio sources. Interestingly, they do not; see, for example, Tovmassian et al. (1999) who studied radio emission in compact groups with a median redshift of 0.09 and a distribution of 1.4-GHz luminosities in the range 8×10^{21}–1×10^{25} W Hz^{-1} with a median of 2×10^{23} W Hz^{-1}. The study found that although radio emission was detected in 20 per cent of compact groups, only 1 per cent of groups contained a potential tailed radio galaxy and none contained two tailed sources even though several galaxies have luminosities greater than J0321−455. Furthermore, one group (ShCG219) containing an FR II type radio galaxy shows evidence for strong interaction with another nearby galaxy of similar magnitude and yet this second galaxy shows no sign of having associated radio emission. These results are hard to account for if the triggering of an AGN occurs simply through galaxy–galaxy interactions.

3.3 Characterizing the motion of the galaxies

Optical imaging and spectroscopy have given us two spatial and one velocity dimension for the host galaxies. Radio imaging has added extra information from which we can infer the transverse motions of the galaxies. We can therefore, albeit crudely, estimate the inclination of the orbital plane to the line of sight.

Under the assumption that J0321−455 is a binary system, the small disparity in their spectroscopically measured redshifts results then from a line-of-sight velocity difference of 180 km s^{-1} where the sources are moving about each other in a clockwise (east through north) direction such that J0321−455S appears blueshifted and J0321−455N redshifted from their common systemic redshift. Assuming the galaxies have equal masses (as determined by their very similar optical magnitudes) we then can infer J0321−455N and J0321−455S to have line-of-sight velocities of 90 and −90 km s^{-1}, respectively.

If the line-of-sight velocity is of the order of the orbital velocity of the binary system, then we can infer an orbital period of 8×10^8 yr. As the two radio sources are neither intertwined nor display significant curvature to the locus of their tails, this orbital period

should be much longer than the radiative age of the synchrotron particles at the edges of the tails. This is consistent with Blundell & Rawlings (2000) who show that the maximum radiative age of a synchrotron emitting particle is a few times 10^7 yr.

A crude alternative to infer the orbital velocity of the binary is to assume that the synchrotron plasma of the radio jets are deposited with no bulk kinetic energy. Then we can assume that the extent of the radio tails represents the host galaxy motion through the IGM. Under this assumption, we infer a minimum orbital velocity of 3000 km s^{-1} if the synchrotron electrons are as old as 5×10^7 yr. The inconsistency between these two velocities forces us to conclude that host galaxy motion cannot be the only contributing factor to the morphology, and extent, of the radio tails. In other words, the morphology of the radio tails must be a combined effect of orbital motion plus another force accelerating them east–west relative to north–south.

The light synchrotron plasma tails of the BT sources are embedded in the denser thermal environment. The dynamical evolution of the filament and, consequently, the tidal expansion of the gaseous environment of the BT sources, might be expected to lengthen the structures east–west relative to north–south and might be the cause of the east–west extensions in the tails from the binary system. In this scenario, the extended western jet of J0321−455S lies ahead of the binary system and therefore has a relatively greater acceleration toward the supercluster than its host galaxy. Similarly, the radio tails of J0321−455N extend behind the binary relative to the supercluster and are accelerated more slowly than the binary system. In this interpretation, the morphology of the BT sources is partly consistent with tidal expansion of the environment along an east–west direction owing to two influences: the proximity (3 Mpc in projection) of the massive ($5 \times 10^{15} - 5 \times 10^{16}$ $M_\odot$) supercluster and the less massive but much closer S345 (10^{13} $M_\odot$ located 0.4 Mpc in projection). A factor of 2 differential expansion of the IGM in east–west relative to north–south would then require about 2×10^8 yr.

3.4 What bends the tails?

There are several factors that might contribute to bending of the tails of BT radio galaxies, and these will probably depend on the environment the sources are located within. Some studies have shown that the bending of BT sources in poor clusters, with typical observed densities of 10^{-4} cm^{-3}, can be produced if the host galaxy is travelling with velocities of the order of 1000 km s^{-1} (Venkatesan et al. 1994; Doe et al. 1995) relative to the ICM gas. This usually means the cluster is virialized, the ICM gas is in hydrostatic equilibrium within the cluster potential, and the galaxies are moving in the cluster potential and relative to the gas. An alternate scenario is one in which the ICM gas has streaming flows driven by changing gravitational potentials in cluster mergers and, as a consequence, the ICM gas may have an associated bulk velocity relative to the potential and the galaxies. In both cases, the bending is inferred to be a result of the deflecting pressure of the ICM, arising from the relative motion of the galaxy and the ICM. With orbital velocities in the order of 100 km s^{-1}, we reject this possibility for the morphology of J0321−455.

Alternatively, a wind would surely bend the tails of both galaxies in the same direction, as seen in other examples of clusters containing several BTs (e.g. the Abell clusters A3266 and A119). The radio images of J0321−455 show that the tails in the two-tailed radio sources trail off in very different directions. Obviously, this cannot be caused by relative motion of the binary as a whole with respect to the ICM.

The *ROSAT* PSPC broadband image detects thermal X-ray gas in the vicinity of the binary and we infer that, if associated with S345 and the radio galaxies, this gas might have a temperature of ∼0.6–1.3 keV (Bird, Mushotsky & Metzler 1995) depending on whether the gas is associated with the binary or the cluster potential. The radio tails have a fairly constant width along their lengths, suggesting static confinement by the ICM thermal gas pressure. Assuming minimum energy conditions (Miley 1980), the synchrotron tails have internal pressures of $\sim 9 \times 10^{-13}$ dyne cm^{-2} indicating an ambient density of 6×10^{-4} cm^{-3}. Models for deflecting jets in low-luminosity sources suggest that the low relative velocity between the host galaxies and the ambient gas, together with the density we infer for the gas, are insufficient to cause the bending via deflecting pressures.

Another factor which may play a role in the observed bending of BTs in clusters is the existence of turbulence in the intracluster gas caused by cluster merger-induced shocks. In this case the cluster is no longer virialized and the gas becomes heated and turbulent, consistent with observations showing that WATs are preferentially located in clusters containing significantly higher levels of X-ray emission than a similar sample of radio-quiet counterparts (Bliton et al. 1998). There are several reasons why we consider that merger-induced 'cluster weather' might play a role in the case of J0321−455. First, the results from Section 2.5 indicate that Abell S345 and the binary probably have a peculiar velocity associated with a gravitational infall into the H–R supercluster. Secondly, there is X-ray evidence suggesting Abell S345 is not a relaxed cluster, but rather is in a dynamically evolving state. Thirdly, S345 and the binary are part of a filamentary structure.

In conclusion, the model we propose is one in which the thermal gaseous environment statically confines the light synchrotron plasma and provides a dense environment (substantiated by the X-ray profile of the group and the collimated radio tails) within which the light radio tails are embedded. The orbital motions of the binary with respect to the relatively static ambient medium, as well as the tidal differential expansion in the ambient gas, have together resulted in the BT morphologies. The tails, therefore, represent the trails of the moving host galaxies within the differentially expanding environment. The detailed paths of the tails would probably be additionally influenced by any turbulence or 'cluster weather' as a consequence of the evolution in the large-scale structure, particularly the differential gravitational acceleration towards the nearby supercluster.

4 SUMMARY

This work has presented a shining example of the influence of large-scale flows on the morphology of radio galaxies. We have presented multiwavelength observations of a pair of tailed radio galaxies located on the periphery of the poor Abell cluster S345, and residing ∼3 Mpc in projection from the H–R supercluster. This system is extraordinary because it is (with the possible exception of 3C 75) the only known example of a binary system of powerful radio galaxies. Although the obvious triggering mechanism for the pair is their mutual interaction, the lack of other examples in the literature is hard to reconcile with such a statement. We suggest that turbulence and tidal forces resulting from the nearby cluster and supercluster may be another consideration. Optical spectroscopy of the host galaxies and their neighbours on the sky show that the hosts constitute a binary system. High-resolution radio imaging has shown that the tails of both galaxies are extended east–west along a galaxy filament linking S345 to the supercluster. Multi-object spectroscopy of

galaxies within a 1° radius shows that S345 and other nearby clusters have a 3D spatial distribution consistent with S345 and the binary being part of a filament that is suffering tidal acceleration towards the nearby H–R supercluster. The existence of an X-ray substructure indicates a lack of dynamical equilibrium and is support for turbulent 'cluster weather' in the gaseous environment. We propose that the BT source structure has evolved primarily as a result of the combined effects of binary orbital motion and tidal differential expansion in the environment over a period of less than 10^8 yr.

ACKNOWLEDGMENTS

These observations would not have been possible without the help of Russell Cannon (AAO) for the 2dF observations and suggestions on the galaxy distribution analysis and the members of the 2dF-GRS team, led by Will Sutherland, whose RUNZ software allowed us to measure the redshifts of the 2dF galaxies. We are grateful to Matthew Colless for the nine-template spectra used for cross-correlation. We thank Lakshmi Saripalli and Ann Burgess for their contributions made early on in this work. We also thank our referee Chris Simpson for his valuable comments. The Australia Telescope is funded by the Commonwealth of Australia for operation as a National Facility managed by CSIRO. This research has also made use of the Astrophysics Data System of NASA and of the NASA/IPAC Extragalactic Data base (NED) which is operated by the Jet Propulsion Laboratory, California Institute of Technology, under contract with the National Aeronautics and Space Administration.

REFERENCES

Abell G. O., Corwin H. G., Olowin R. P., 1989, ApJS, 70, 1
Ashman K. A., Bird C. M., Zepf S. E., 1994, AJ, 108, 2348
Barton Gillespie E., Geller M. J., Kenyon S. J., 2003, ApJ, 582, 668
Bird C. M., Mushotsky R. F., Metzler C. A., 1995, ApJ, 453, 40
Bliton M., Rizza E., Burns J. O., Owen F. N., Ledlow M. J., 1998, MNRAS, 301, 609
Blundell K. M., Rawlings S., 2000, AJ, 119, 1111
Byrd G., Valtonen M., 1990, ApJ, 350, 89
Colless M., 1998, in Wide Field Surveys in Cosmology, Early Results from the 2dF Galaxy Redshift Survey. Editions Frontieres, Gif-sur-Yvette, p. 77
Dalton G. B., Maddox S. J., Sutherland W. J., Efstathiou G., 1997, MNRAS, 289, 263
den Hartog R., 1997, MNRAS, 284, 286
Doe S. M., Ledlow M. J., Burns J. O., White R. A., 1995, AJ, 110, 46
Fanaroff B. L., Riley J. M., 1974, MNRAS, 167, 31P
Gladders M. D., Yee H. K. C., 2000, AJ, 120, 2148
Gomez P. L., Pinkney J., Burns J. O., Wang Q., Owen F. N., Voges W., 1997, ApJ, 474, 580
Griffith M. R., Wright A. E., Burke B. F., Ekers R. D., 1994, ApJS, 90, 179
Hardcastle M. J., Sakelliou I., 2004, MNRAS, 349, 560
Hickson P., 1997, ARA&A, 35, 357
Lim J., Leon S., Combes F., Dinh-V-Trung, 2000, ApJ, 545, L93
Miley G., 1980, ARA&A, 18, 165
Peacock J. A., Cole S., Norberg P., Baugh C. M. E. A., 2001, Nat, 410, 169
Rose J. A., Gaba A. E., Christiansen W. A., Davis D. S., Caldwell N., Hunstead R. W., Johnston-Hollitt M., 2002, AJ, 123, 1216
Saripalli L., Subrahmanyan R., Hunstead R. W., 1994, MNRAS, 269, 37
Sault R. J., Killeen N. E. B., 1999, Miriad User's Guide. Available from http://www.atnf.csiro.au/computing/software/miriad
Tonry J., Davis M., 1979, AJ, 84, 1511
Tovmassian H. M., Chavushyan V. H., Verkhodanov O. V., Tiersch H., 1999, ApJ, 523, 87
Venkatesan T. C. A., Batuski D. J., Hanisch R. J., Burns J. O., 1994, ApJ, 436, 67

This paper has been typeset from a TEX/LATEX file prepared by the author.